WORLD CONFERENCE ON TIMBER ENGINEERING 2025
BRISBANE, AUSTRALIA

Advancing Timber for the Future Built Environment

GLUED-IN HARDWOOD RODS AS REINFORCEMENT FOR GLULAM UNDER COMPRESSION PERPENDICULAR TO THE GRAIN

Yue Wang[1], Roberto Tomasi[2], Angelo Aloisio[3], Roberto Crocetti[4], Tianxiang Wang[5]

ABSTRACT: For the design of high-rise timber buildings, the accumulation of self-mass and the resultant permanent deformation is a critical matter, especially at the occurrence of compression perpendicular to the grain (CPG). Metal fasteners, e.g., self-tapping screws, are conventional reinforcements against CPG deformation in timber members, and the relevant measures have been standardized in the new version of EC5. This study investigates the technique of utilizing glued-in wooden rods and laminated densified wooden (LDW) rods as CPG reinforcements. Test series are first planned to characterize the single-fastener behavior by applying direct loading on the single rod. Thereafter, the global behavior of reinforced glulam specimens, following the loading of Case A and Case B as defined by prEC5, are respectively investigated. Possible associated failure modes are planned to be observed and then classified to propose analytical prediction formulas. The numbers of glued-in wooden rods also varied on the specimen geometry to investigate if the effective numbers are applicable when applying multiple fasteners. Digital image correlation measurements were also conducted on featured Case B specimens to visualize the dispersion of stress and the effect of reinforcing wooden rods.

KEYWORDS: Wooden rod, laminated densified wooden rod, compression perpendicular to the grain, reinforcement.

1 – INTRODUCTION

Self-mass accumulation and the resultant permanent deformation are critical in high-rise timber structures. Given timber's weak cross-grain properties, the large permanent deformation is non-negligible in the case of compression perpendicular to the grain (CPG) [1]. CPG failure is especially crucial when designing timber components that are mainly intended to withstand local compression forces, such as beam-column joints or column-panel joints in mass timber buildings.

Metal fasteners, e.g., self-tapping screws, are conventional reinforcements against CPG deformation in timber members. Attributed to the pioneering work by Blaß and Schmid [2] and Blaß and Bejtka [3], the screw-reinforcing technique has been standardized in prEurocode 5 [4].

However, it is worth noting that the extensive use of metallic parts entails high energy consumption and CO_2 emissions [5]. As timber structures scale up, the quantity of entailed metal proportionally increases, trading off timber structures' merits being lightweight and carbon neutral. For instance, the four-story Lisbjerg Hill House in Denmark consumed over 18000 screws, significantly adding to the building's cost, weight, and carbon footprint [6].

As compared to screw reinforcements, glued-in wooden rods possess the potential to provide a more lightweight and environmentally friendly solution. More importantly, it also provides a high-value use of hardwood (e.g., beech and birch), which is usually used for generating heat. Besides, using wooden rods as fasteners can avoid the potential collision between metal reinforcements and metal fasteners during the erection of connections.

[1] Yue Wang, Department of Civil and Architectural Engineering, KTH Royal Institute of technology, Stockholm, Sweden, yue4@kth.se

[2] Roberto Tomasi, Faculty of Science and Technology, Norwegian University of Life Sciences, Norway, roberto.tomasi@nmbu.no

[3] Angelo Aloisio, Department of Civil, Construction-Architectural and Environmental Engineering, Università degli Studi dell'Aquila, Italy, angelo.aloisio1@univaq.it

[4] Roberto Crocetti, Department of Civil and Architectural Engineering, KTH Royal Institute of technology, Stockholm, Sweden, crocetti@kth.se

[5] Tianxiang Wang, Department of Civil and Architectural Engineering, KTH Royal Institute of technology, Stockholm, Sweden, tiawan@kth.se

https://doi.org/10.52202/080513-0408

The technique of glued-in wooden rods as reinforcements is documented in the literature. Conway et al. utilized thermo-mechanical densified wood manufactured from Scots Pine (*Pinus Sylvestris*) to reinforce glulam specimens against CPG [7,8]. Densified wooden dowels with a diameter of 10 mm were adopted, with the arrangement numbers varying from 2 to 4 to 6. Parallel test series with self-tapping screws were also conducted. As a result, although the densified wooden dowels are not outperforming the metal screws, a 16% compressive strength increase was reported for specimens reinforced with 2 densified wood dowels and a 30% increase was reported for those with 6 densified wood dowels. Such reinforcing techniques were modelled in ABAQUS/Explicit, adopting cohesive zone modelling (CZM) and Hill plastic yield criterion [9].

This study reveals the technique of utilizing glued-in hardwood (birch) rods and laminated densified wooden (LDW; beech) rods as local reinforcements for glulam members loaded in CPG. The so-called 'single fastener' behavior was first characterized by only applying axial compression on the glued-in rods (Figure 1a). After that, the global behavior of reinforced glulam elements was studied. Eurocode 5 defined different loading cases for CPG. This study addressed the first two, namely, Case A and Case B, as illustrated in Figures 1b and 1c.

2 – MATERIALS AND METHODS

This study exclusively utilized glulam with a strength grade of GL30c and an average density of 463.0 kg/m3, supplied from Moelven AB (Töreboda, Sweden). The equilibrium moisture content (MC) is measured to be 10.0% following the oven-dry method described in EN 322 [10].

Two types of wooden rods were utilized, i.e., dowels made of solid birch and lignin-densified wood (LDW). Throughout this study, they are respectively referred to as the 'Birch rod' and the 'LDW rod.' The utilized LDW dowels, Lignostone®, are laminated, densified wood products made from red beech. The beech veneers are combined with high temperatures and bonded by a curable synthetic resin. As a result, the fibers are flattened and fused, yet the cell wall is still intact.

The density of both wooden rods was calculated by dividing each part's weight by its nominal volume. As a result, the birch rod possesses a density of 608.3 kg/m^3 and an MC of 7.7%, and the LDW rod possesses a density of 1334.8 kg/m^3 and an MC of 5.0%. Each rod has a diameter of around 20 mm.

The assembly process of glue-in wooden rods is consistent regardless of the test configurations. The wooden rods (birch or LDW) were first cut into the desired lengths during the assembly. The glulam was then drilled with a diameter of 22 mm, obtaining an adhesive layer thickness of around 1 mm. The drilling depth is monitored according to the specimen specification.

After that, the adhesive was mixed with the hardener with a stoichiometric volume ratio of 2:1. The adhesive utilized is a two-component epoxy adhesive XEPOX-F (fluid) from Rothoblaas®, which is favored for its low viscosity, making it relatively easy to pour into predrilled holes. The rods were spined by hand while being pressed in to avoid any occurrence of air voids inside. Thereafter, the wooden rods were pressed into the holes. and placed in a fume hood until the adhesive was fully cured. Figure 1d illustrates the whole assembly process of glued-in wooden rods.

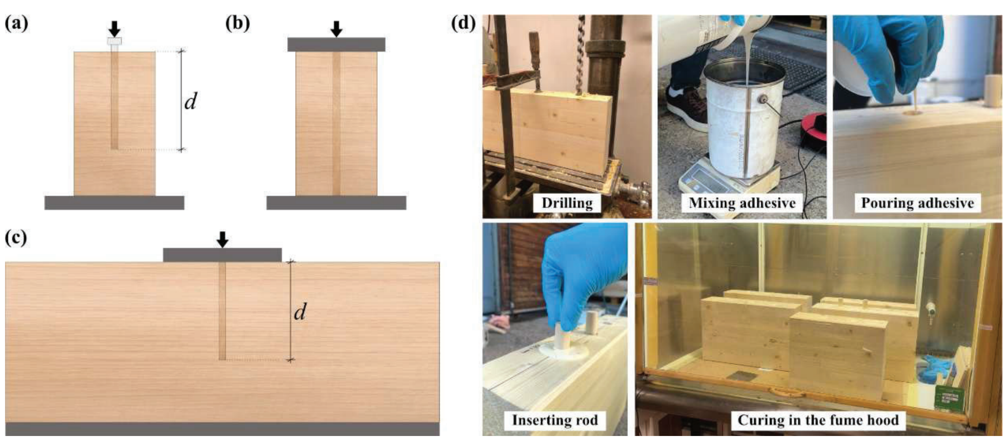

Figure 1. Illustration on the a) single fastener test, b) Case A CPG test, c) Case B CPG test, and d) assembly process of glued-in wooden rods: from drilling, mixing adhesives, pouring adhesive in predrilled holes to inserting rods and curing adhesives.

https://doi.org/10.52202/080513-0408

2.1 SINGLE FASTENER TEST

Inspired by the 'Torx' apparatus in the work of Aloisio et al. [11], a specialized loading head with a diameter of 22 mm (dowel plus adhesive layer thickness) was adopted to apply direct loading on a single glued-in wooden rod (Figure 2a). A GL30c glulam beam with a cross-section of 90 mm × 270 mm was first cut into short lengths of 400 mm to accommodate 3 test replicates for wooden rods.

By varying the glued-in depth (denoted as d) of birch or LDW rods in the single fastener test, all possible associated failure modes are planned to be revealed. The number of test replicates and penetration depth for all planned configurations are summarized in Table 1.

Table 1: Test configurations for studying the single-rod behavior

Rod type	Rod penetration depth *d* (mm)					
	70	105	140	175	210	245
Birch rod	3	3	3	3	3	3
LDW rod	3	3	3	NAN	3	NAN

Prior to the experiments, the upper surfaces of specimens were planned to remove excessive adhesive and create a smooth surface. All tests were conducted at NMBU Norwegian University of Life Sciences (Ås, Norway) on a ZwickRoell Z1200 universal testing machine. A supplementary fixture was tailored for transmitting loads from the piston onto the rods, as in Figure 2b.

Hagen [12] conducted similar tests on screws and reported non-negligible internal deformations from the unreinforced portion of glulam underneath the wooden rod. Therefore, in this study, angle brackets were attached to the tip location of wooden rods (Figure 2b). Two LVDTs were fixed on the bottom platen, and their probes were attached to the angle bracket so that the movement of the glulam at the wooden rod tips was monitored. The piston head displacement subtracting the LVDT readings was regarded as the true slip measurement of the fastener.

The loading protocol followed guidelines given in the standard ISO 6891 [13], which mandates that the test shall be executed based on an estimated force F_{est}, which is based on the trial test. The detailed loading steps are presented in Figure 3.

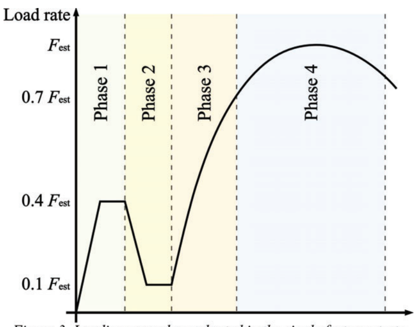

Figure 3. Loading procedure adopted in the single fastener tests.

Moreover, supplementary compression tests were also conducted on birch and LDW rods to characterize their capacity and failure modes under pure compression. The apparatus is presented in Figure 4.

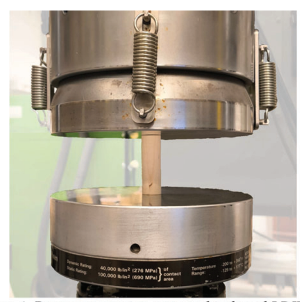

Figure 4. Pure compression tests on birch and LDW rods.

The results from pure compression tests will be compared and discussed with single fastener tests in Section 3.1.

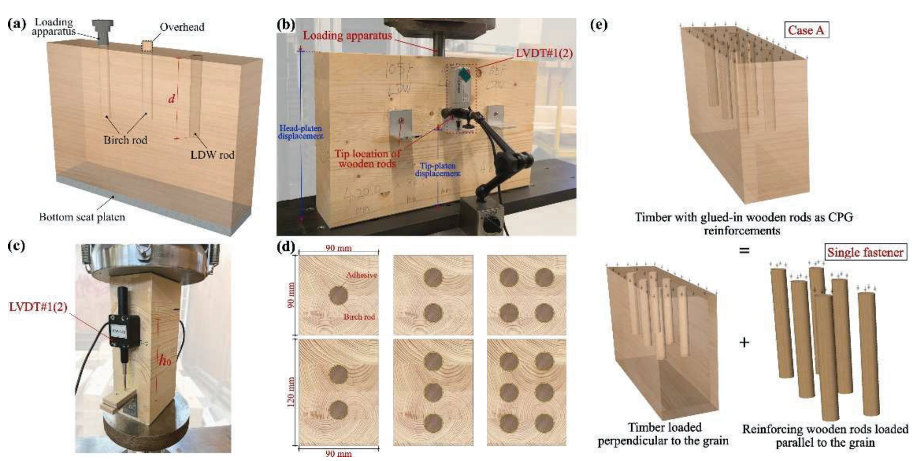

Figure 2. Illustration on the apparatus and configuration of a) b) single fastener test, c) d) Case A CPG test, and d) hypothesized loading mechanism.

2.2 'CASE A' CPG SPECIMEN TEST

Case A refers to when CPG specimens were subjected to uniform compression forces across the cross-section. As in Figure 2c, a spherical bearing platen was mounted on the test machine to ensure full contact with the specimen. The compression force was applied following the guidelines in EN 408 [14]. The loading rate was controlled to be 1 mm/min, so the maximum load could be reached within a relatively short time (3 to 7 minutes, as in EN 408).

Two linear variable differential transformers (LVDTs) were installed on the sides of the Case A glulam specimen. The measured range (h_0) is 170 mm, around 60% of the specimen's total height (270 mm). As in Figure 5, the piston load is plotted versus the average LVDT readings. The capacity is defined as the intersection point between the test curves and the linear portion offset by $0.01 \cdot h_0$.

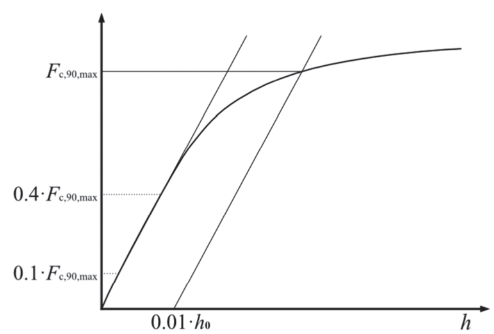

Figure 5. Determination of the maximum load $F_{c,90,max}$ according to EN408.

The glulam cross-section, number of glued-in rods, rod species, and test replicates regarding 'Case A' specimens in this study are summarized in Table 2.

Table 2: Configurations and test replicates of 'Case A' specimens.

Glulam cross-section	Number of rods	Rod species	Test replicates
90 mm × 90 mm	n = 1, 2, 4	Birch rods	3
120 mm × 90 mm	n = 2, 3, 6		3

As in Figure 2d, two different cross-sections (90 mm × 90 mm; 120 mm × 90 mm) were adopted to create geometrical variability. Besides, the amount of glue-in rods varied from 1 to 2 to 4 to 6 to investigate the significance of effective numbers as per the 'group effect.' Unreinforced glulam pieces were also tested as a reference.

It is also worth noting that the rods shall always have the same length as the glulam thickness for Case A specimens. Otherwise, the unreinforced portion of the glulam underneath the rod tip will be the 'weakest link', and the measured corresponding capacity will be close to the CPG strength of unreinforced glulam material.

Besides, as illustrated in Figure 2e, the loading mechanism of a reinforced 'Case A' glulam specimen is hypothesized as the summation of two portions, namely, 1) the unreinforced glulam being loaded under CPG and 2) the reinforcing rods being loaded parallel to the grain. This hypothesis will be examined later using capacity results from the single fastener tests and Case A specimen tests.

2.3 'CASE B' CPG SPECIMEN TEST

A 'Case B' specimen refers to a short glulam beam being locally loaded on one side (usually the top) but evenly supported on the other (usually the bottom). In this study, a steel plate (90 mm × 90 mm) was placed on top and transmitted the local compression force, as in Figure 6c.

Glulam beams with the strength grade of GL30c and a cross-section of 90 mm × 270 mm were cut into short lengths of 650 mm. This length considers the summation of the steel plate width (90 mm) and the 45° load-dispersion angle (270 mm × 2). The loading was applied in a displacement-controlled manner at a rate of 6 mm/min, so the maximum capacity was reached within 5 to 10 minutes after the onset of the experiments.

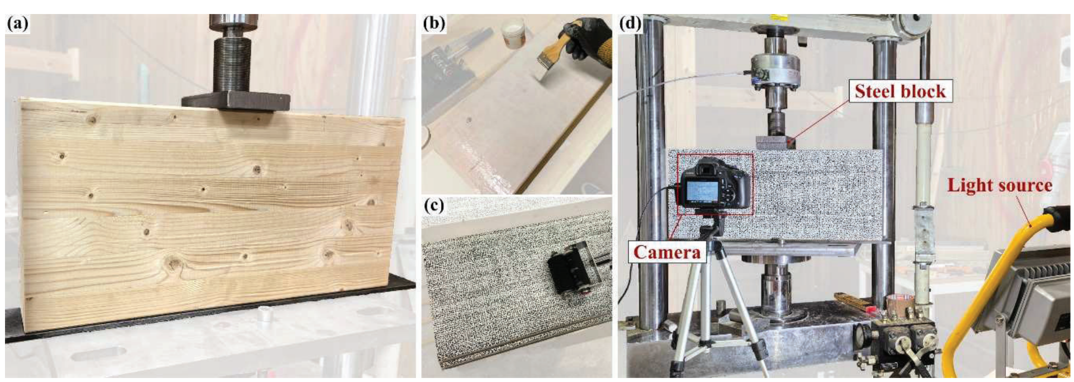

Figure 6. Illustration on the a) single fastener test, b) Case A CPG test, c) Case B CPG test, and d) assembly process of glued-in wooden rods: from drilling, mixing adhesives, pouring adhesive in predrilled holes to inserting rods and curing adhesives.

https://doi.org/10.52202/080513-0408

The tested configurations of 'Case B' specimens in this study are summarized in Table 3.

Table 3: Configurations and test replicates of 'Case B' specimens.

Glulam cross-section	Rod	Number of rods	Penetration depth (mm)	Test replicates
90 mm × 270 mm × 650 mm	Birch	*n* = 1 or 2	70, 140, 210	2
	LDW	*n* = 1	70	2

Moreover, for Case B specimens specifically, digital image correlation (DIC) measurements were conducted to capture the full-field displacement and strain contour. The inspection surface of featured Case B specimens was first white painted (Figure 6a), and stochastic speckles were generated using a roller with black oli paints (Figure 6b).

An LED light (Figure 6c) was set to eliminate shadows and interference with the measurements. A camera was set on a tripod, and pictures were taken at intervals every 3 seconds. The open-source DIC package Ncorr [15] in Matlab R2024 [16] was adopted to post-analyze the pictures.

3 – RESULTS AND DISCUSSIONS

3.1 'SINGLE FASTENER' TEST

The piston load-calibrated displacement curves for all 'single fastener' specimens are presented in Figure 7a. The dashed lines stand for birch rods with lengths varying from 70, 105, …, 240 mm. Despite the variation in lengths, the specimens yielded similar ultimate capacities from 24.7 to 30.2 kN, with the average capacity being 27.5 kN.

The solid lines stand for LDW (laminated densified wooden) rods with lengths of 70, 105, 140, and 210 mm. As the rod lengthened, the measured single fastener capacity escalated from 45.4 to 60.7 to 70.4 to 73.7 kN.

Figure 7b summarizes the failure modes for typical 'single fastener' test specimens. It is worth noting that after the specimens' failure, the rods were pushed further for another 5 or 15 mm, making the failure modes more visible.

For short LDW rods, the capacity of the adhesive layer is lower than the compressive resistance of the rods itself. As a result, an adhesive failure was initiated as shear cracks inside the adjacent glulam. Once loaded further (15 mm), the entire adhesive layer peeled off, and the bottom part of the rod, together with the glulam underneath, was compressed. For long LDW rods, the capacity of the adhesive layer gradually reaches and surpasses the rods' compressive resistance, converging in compressive failure. As the rod was loaded further to 15 mm, the LDW matrix was crushed and skewed to the side. For birch rods, regardless of the penetration depth, the failure always occurs as compression failure inside the wooden rods located close to the loading head. This is verified by the similar failure capacities among specimens with different rod insertion lengths in Figure 7a.

Figure 8 presents the results from pure compression tests, which gave the birch rods and LDW rods an average capacity of 17.6 kN and 47.0 kN, respectively.

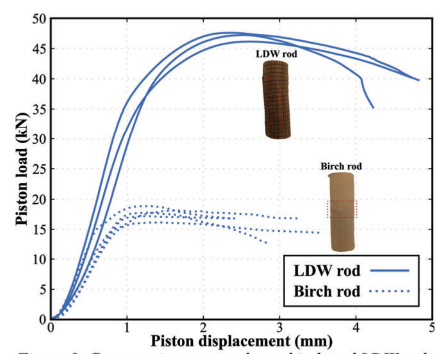

Figure 8. Compression test results on birch and LDW rods.

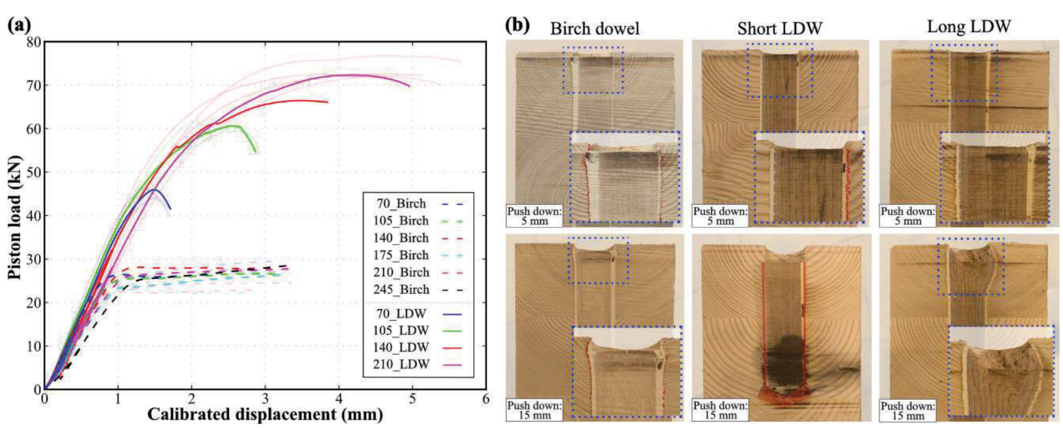

Figure 7. a) Piston load-calibrated displacement curves for single fastener tests on birch and LDW rods, and b) corresponding failure modes when pushing short or long dowels further for 5 mm or 15 mm.

The 'single fastener' capacities for birch and LDW rods (Figure 7) are both higher than their pure compression capacities (Figure 8), which is attributed to the 'confinement effect' brought by the surrounding glulam substrate and adhesive layer.

3.2 'CASE A' CPG SPECIMENS

The recorded piston loads when testing Case A specimens were transformed into compressive stress following:

$$\sigma_{c,90,\mathrm{CaseA}} = F_{\mathrm{piston}} / (w \cdot b) \qquad (1)$$

where w and b are the specimens' width (90 mm) and breadth (90 or 120 mm). And the compressive strain is simply the LVDT readings (δ) divided by the measuring gauge length (170 mm).

For each specimen, the reinforcement ratio is defined as the summated rods' area divided by the specimens' cross-sectional area. As a result, the stress-strain curves for 'Case A' specimens are presented in Figure 9a. According to guidelines given in EN 408, the capacities for 'Case A' specimens were evaluated as the 1% strain offset intersection points. The capacity and strength values of all investigated Case A specimens are summarized in Table 4.

Table 4: Reinforcing ratio, capacity, and strength data of all investigated 'Case A' specimens.

Case A Configuration	Reinforce ratio	Average capacity (kN)	Average strength (MPa)
Unrein	0%	32.8 (1.2)	3.1 (0.1)
R1_90	4.7%	50.2 (3.6)	6.3 (0.4)
R2_120	7.0%	84.1 (4.5)	8.0 (0.5)
R2_90	9.4%	82.1 (9.5)	10.4 (1.1)
R3_120	10.6%	111.3 (2.3)	10.6 (0.2)
R4_90	18.8%	130.8 (7.6)	16.5 (1.0)
R6_120	21.1%	188.9 (2.4)	17.8 (0.3)

Several observations can be highlighted in Figure 9a. First, compared to unreinforced glulam specimens (3.1 MPa; black curves), all reinforced specimens (colored curves) depicted a much stiffer behavior in the initial loading phase. Besides, specimens reinforced with glued-in rods showed significantly enhanced CPG strength values. This strength enhancement showed a positive correlation with the reinforcement ratios. When the reinforcement ratios steply increase from 4.7% to 21.1%, the yield capacity increases from 50.2 kN to 188.9 kN, and the equivalent CPG strength increases from 6.3 MPa to 17.8 MPa.

As in Figure 9b, globally, most Case A specimens failed with either: 1) cracks initiated in the middle of specimens or 2) skewing of specimens adjacent to the supports. When cutting the failed specimens, it was observed that most failures occurred as the compressive crushing of birch rods.

Given that the average single fastener capacity of birch rods is 27.5 kN. For a specific configuration with the glulam cross-section of $w \times b$ and n rods. The glulam capacity is calculated as the net area times the materials's compressive strength perpendicular to the grain:

$$R_{\mathrm{glulam,net}} = (w \cdot b - n \cdot \frac{\pi \cdot (d+t)^2}{4}) \cdot f_{c,90} \qquad (2)$$

where d is the wooden rod diameter (20 mm), t *is* the adhesive layer thickness (2 mm), $f_{c,90}$ is taken from the test results in Table 4, namely, 3.1 MPa.

The capacity of a reinforced Case A glulam specimen, following the hypothesis in Figure 2e, is the summation of the net glulam resistance and the rod's resistance:

$$R_{\mathrm{glulam,reinforced}} = R_{\mathrm{glulam,net}} + R_{\mathrm{rod,single}} \cdot n \qquad (3)$$

where $R_{\mathrm{rod,single}}$ is the single fastener capacity, the average value of which is determined as 27.5 kN for birch rods.

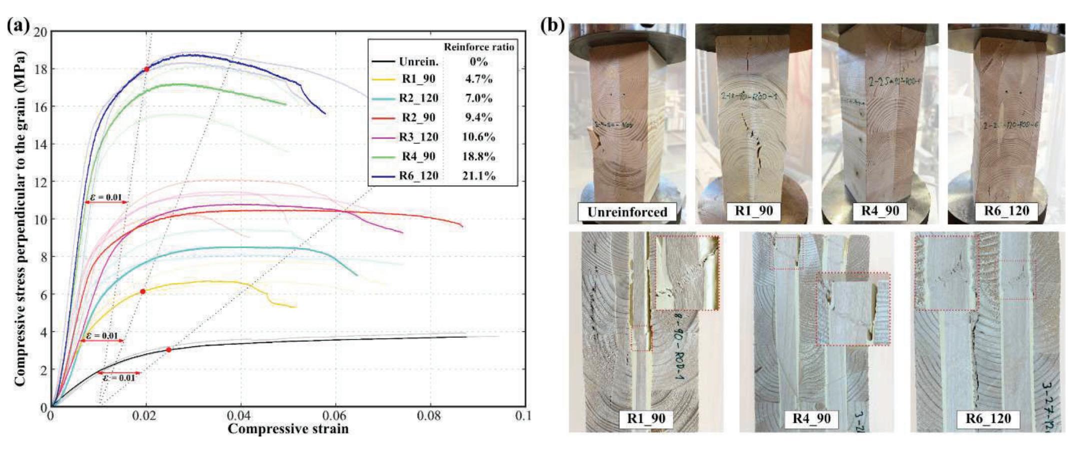

Figure 9. a) Stress-strain curves for Case A specimens with varying geometry and reinforcing ratios. b) Failure modes for typical Case A specimens.

https://doi.org/10.52202/080513-0408

The correlation between the predicted capacity obtained via Equations 1-3 and the measured capacity (presented in Table 4) is plotted in Figure 10. The red-dotted line is a diagonal line with a slope of 1:1, which represents an ideally perfect correlation.

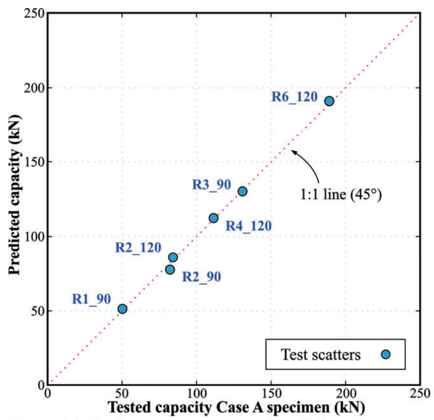

Figure 10. Prediction versus test results of Case A specimens.

Figure 10 shows that for Case A specimens, the predicted capacity values correlate well with the experimental values.

This observation validates the proposed hypothesis that the capacity of a reinforced 'Case A' glulam specimen can be calculated as the summation of 1) the capacity of an unreinforced glulam beam loaded under CPG, and 2) the capacity of wooden rods loaded parallel to the grain direction (mechanism illustrated before in Figure 2e). Moreover, such a hypothesis performed robustly when predicting specimens with two different cross-sections.

3.3 'CASE B' CPG SPECIMENS

During the test of Case B specimens, the recorded piston loads were transformed into compressive stress following:

$$\sigma_{c,90,\mathrm{CaseB}} = F_{\mathrm{piston}} \,/\, (w_{sp} \cdot b_{sp}) \qquad (4)$$

where w_{sp} and b_{sp} are the steel plates' width (90 mm) and breadth (90 mm). The compressive strain is the recorded displacement divided by the specimen height (270 mm).

The stress-strain curves for all Case B specimens are presented in Figure 11. To avoid the curves interweaving with each other, the curves for specimens reinforced with one rod are presented in Figure 11a, and those for specimens with two rods are presented in Figure 11b.

Several observations shall be highlighted in Figures 11a and 11b. First, intuitively, the general trend is that the more wooden dowels are glued in, and the deeper they are embedded, the stronger the reinforcement effect is. This is reflected in the presented curves. Second, with the increase in glued-in rod numbers and glued-in depth, the initial stiffness of loaded specimens also escalated. However, no significant difference was depicted in terms of the stiffness values in the strain-hardening loading phase.

Moreover, it is worth noting that for specific specimens, load drop was observed prior to the strain-hardening phase due to the premature cracks initiated from the edge of specimens. The pre-cracks are presented as red-colored regions on the edge of specimens in Figure 11c.

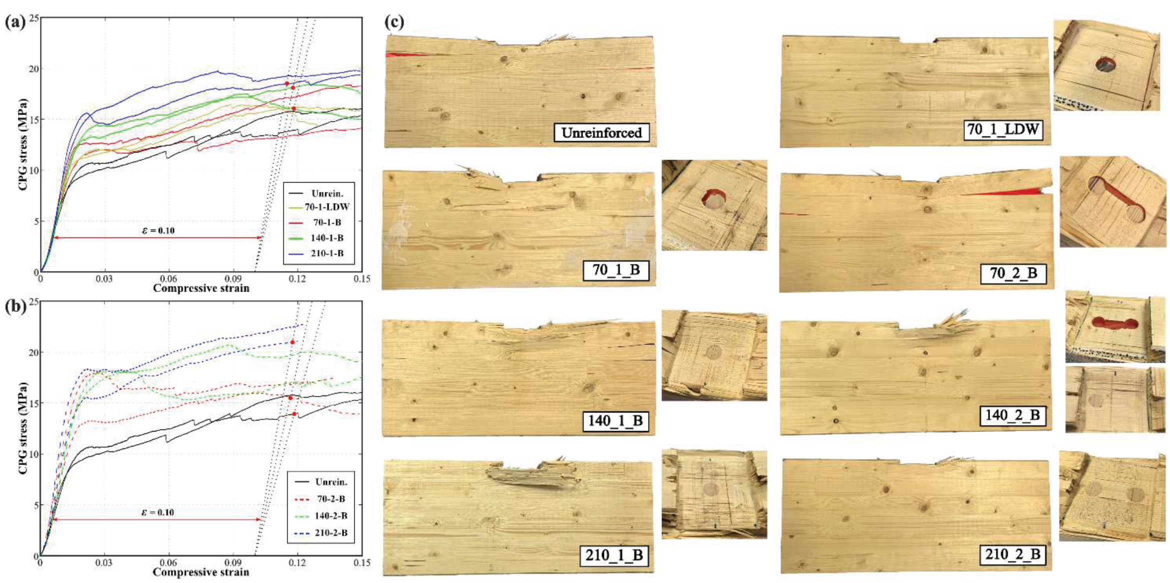

Figure 11. Stress-strain curves of Case B specimens reinforced with a) one glued-in rod, b) two glued-in rods, and c) failure modes of all specimens.

Besides, for specific configurations, namely 70_1_LDW, 70_1_B, 70_2_B, and 140_2_B, failure in the adhesive layer was observed, which is marked as the red region in Figure 11c. This phenomenon is attributed to a weak adhesive layer capacity, as it only occurs on short rods. Another possible explanation is insufficient quality control during the drilling process (excessive sawn dust remained in holes) or the curing process of the adhesive.

Table 5 summarizes the measured corresponding capacity and strength data of all investigated Case B specimens. The number within the parathesis represents the standard deviation.

Table 5: The capacity and strength data of all 'Case B' specimens.

Case B Configuration	Average capacity (kN)	Average strength (MPa)
Unreinforced	120.2 (10.6)	14.8 (1.3)
70-1-LDW	129.0 (2.6)	15.9 (0.3)
70-1-B	123.8 (20.9)	15.3 (2.6)
140-1-B	138.2 (11.7)	17.1 (1.4)
210-1-B	152.9 (4.2)	18.9 (0.5)
70-2-B	131.3 (8.2)	16.2 (1.0)
140-2-B	148.4 (15.9)	18.3 (2.0)
210-2-B	177.1 (10.0)	21.9 (1.2)

Several comments can be addressed as per the results in Figure 11 and Table 5. First, comparing the 70-1-LDW and the 70-1-B groups in Figure 11a, the former seemed to have a lower capacity in the initial loading phase, which is attributed to the premature adhesive failure of LDW ones (Figure 11c). However, as the loading continued and the displacement enlarged, the LDW group also showed a more significant hardening phase, which is mainly attributed to its stronger material essence (shown previously in Figure 8). That also explains the higher capacity of the 70-1-LDW group in Table 5.

Besides, for Case B specimens, one glued-in 70 mm rod can only enhance the capacity by 3.2%. Elongating the rod to 140 mm and further to 210 mm increases this enhancement to 15.0% and 27.2%, respectively. Increasing the rod number to 2, an enhancement of 9.2%, 23.5%, and 47.3% were observed for 70 mm, 140 mm, and 210 mm rods, respectively. This suggests that the reinforcement effect is only significant for Case B loading case when the rod penetration is sufficiently deep (i.e. 210 mm). The number of rods also enhances the capacity but to an insignificant extent.

Figure 12 presents the contour plots from digital image correlation (DIC) measurements. Strain contours for typical configurations unreinforced glulam, 70-1-B, 140-1-B, 140-2-B, 210-1-B, and 210-2-B are respectively presented in Figure 12a-12f. Fictitious wooden rods are also plotted to better interpret the observations.

First, a clear stress dispersion away from the loaded region can be observed on unreinforced specimens in Figure 12a. This coincides well with the 45° dispersion angle (the cyan dotted lines) suggested by prEurocode 5 [4].

Proceeding to Figures 12b, 12c, and 12e, where the glued-in depth of the rod is 70 mm and 140 mm, the strain dispersion is not significantly different from the unreinforced case. This indicates that regardless of the number of rods, the reinforcement effect is rather limited when the rods are not deeply penetrating the glulam.

Further, in Figures 12e and 12f, where the glued-in depth of rods is 210 mm, the rods are able to 'absorb' most of the elastic compressive strain (blue contours). This verifies the observations in terms of the capacity mentioned before, namely that the reinforcement is only significant when the rod penetration is as deep as 210 mm.

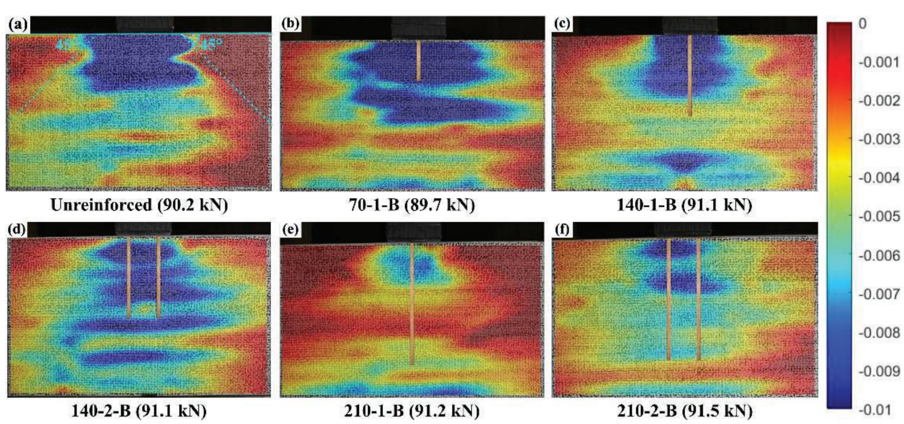

Figure 12. Full-filed strain contour of Case B specimens from DIC measurements for the configurations: a) unreinforced, b) 70-1-B, c) 140-1-B, d) 140-2-B, e) 210-1-B, and f) 210-2-B. The numbers within the parenthesis indicate the corresponding piston loads.

https://doi.org/10.52202/080513-0408

It is worth noting that in this study, no analytical loading mechanism as in Case A specimens was summarized for Case B specimens, which is regarded as future work.

4 – CONCLUSIONS

This study reveals the utilization of glued-in wood rods as CPG reinforcement for glulam elements.

First, the single fastener behavior was characterized by applying compression force solely on the glued-in wooden rods, e.g., birch rods and LDW (laminated densified wooden) rods. For birch rods, regardless of the penetration depth, the failure always occurs as compression failure inside the wooden rods adjacent to the loading head, giving an average capacity of 27.5 kN. For LDW rods, the failure modes are dependent on the capacity magnitude of the adhesive layer and the rods' compressive resistance. Adhesive failure occurs in the case where the former is lower, and compression failure occurs otherwise.

Second, 'Case A' specimens were manufactured and tested. As a result, the unreinforced glulam has a CPG strength of 3.1 MPa. For the reinforced ones, as the reinforcing ratio increases from 4.7% to 21.1%, the yield capacity significantly increases from 50.2 kN to 188.9 kN, and the equivalent CPG strength is enhanced from 6.3 MPa to 17.8 MPa. Besides, the Case A loading mechanism is hypothesized as the glulam loaded cross-grain plus the wooden rods loaded parallel to the grain. This hypothesis is validated by correlating the analytical predictions with the experimental capacity values.

Third, 'Case B' specimens were investigated, and it was found that the reinforcing effect from wooden rods is only significant when the rod penetration is sufficiently deep. Specifically, one glued-in 70 mm rod can only enhance the capacity by 3.2%. Elongating the rod to 140 mm and further to 210 mm increases this enhancement to 15.0% and 27.2%, respectively. Increasing the rod number to 2, an enhancement of 9.2%, 23.5%, and 47.3% were observed for 70 mm, 140 mm, and 210 mm rods, respectively.

Moreover, the full-field strain contour of Case B configurations was captured via digital image correlation (DIC) measurements. As a result, the stress dispersion angle of 45° recommended by prEurocode 5 for Case B loading was visualized. And it was found that when the glued-in depth of rods is as deep as 210 mm, the rods are able to 'absorb' most of the elastic compressive strain. This also cross-validates the observations in terms of the capacity mentioned before.

Several points are listed as limitations or future works. First, no analytical loading mechanism as in Case A specimens was summarized for Case B specimens. Second, discussions on measured stiffness values shall be summarized, and analytical models shall be conducted to better interpret the observations. Third, more parametric experimental schemes shall be supplemented to enhance the robustness of conclusions.

5 – REFERENCES

[1] D.P. Pasca, F.M. Massaro, Y. De Santis, H. Stamatopoulos, J. Ljungdahl, A. Aloisio, Deformation level and specimen geometry in compression perpendicular to the grain of solid timber, GLT and CLT timber products, Eng. Struct. 321 (2024) 118972.

[2] H.J. Blaß, M. Schmid, Self-tapping screws as reinforcement perpendicular to the grain in timber connections, in: PRO 22 Int. RILEM Symp. Joints Timber Struct., RILEM Publications, 2001: p. 163.

[3] H.J. Blass, I. Bejtka, Reinforcements perpendicular to the grain using self-tapping screws, in: Proc. 8th World Conf. Timber Eng., 2004: pp. 233–238.

[4] European Committee for Standardisation (CEN), Draft EN 1995-1-1 Eurocode 5 - Design of timber structures, 2023.

[5] T.E. Norgate, S. Jahanshahi, W.J. Rankin, Assessing the environmental impact of metal production processes, J. Clean. Prod. 15 (2007) 838–848.

[6] A. Dodoo, T. Nguyen, M. Dorn, A. Olsson, T.K. Bader, Exploring the synergy between structural engineering design solutions and life cycle carbon footprint of cross-laminated timber in multi-storey buildings, Wood Mater. Sci. Eng. 17 (2022) 30–42.

[7] C. O'Ceallaigh, M. Conway, S. Mehra, A.M. Harte, Modified wood as compression reinforcement of timber perpendicular to the grain, in: World Conf. Timber Eng. 2021, WCTE 2021, Santiago, Chile, 2021.

[8] M. Conway, S. Mehra, A.M. Harte, C. O'Ceallaigh, Densified wood dowel reinforcement of timber perpendicular to the grain: a pilot study, J. Struct. Integr. Maint. 6 (2021) 177–186.

[9] C. O'Ceallaigh, M. Conway, S. Mehra, A.M. Harte, Numerical Investigation of Reinforcement of Timber

https://doi.org/10.52202/080513-0408

Elements in Compression Perpendicular to the Grain using Densified Wood Dowels, Constr. Build. Mater. 288 (2021) 122990.

[10] European Committee for Standardization (CEN), EN 322 Wood-based panels –Determination of moisture content, 1993.

[11] A. Aloisio, Y. De Santis, M. Pelliciari, M.M. Rosso, M. Fragiacomo, R. Tomasi, Buckling capacity model for timber screws loaded in compression: Experimental, analytical and FE investigations, Constr. Build. Mater. 379 (2023) 131225.

[12] K.M. Hagen, Two-sided reinforcement of CLT and push-in capacity of fully threaded screws, Norwegian University of Life Sciences, 2024.

[13] The International Organization for Standardization, Timber Structures - Joints made with mechanical fasteners - General principles for the determination of strength and deformation characteristics, 1983. https://standards.iteh.ai/catalog/standards/sist/d256e01d-014c-4175-8eee-.

[14] CEN European Committee for Standardization, EN 408:1995 Timber structures - Structural timber and glued laminated timber - Determination of some physical and mechanical properties, 1995.

[15] J. Blaber, B. Adair, A. Antoniou, Ncorr: open-source 2D digital image correlation matlab software, Exp. Mech. 55 (2015) 1105–1122.

[16] MathWorks Inc, Matlab R2024, (2024). https://au.mathworks.com/products/matlab.html.

 https://doi.org/10.52202/080513-0408